MICROWAVE-INDUCED THERMO-ACOUSTIC TOMO-GRAPHY SYSTEM USING TRM-PSTD TECHNIQUE

Guoping Chen[1, 3, *], Xin Wang[1], and Qinghuo Liu[2, 3]

[1]College of Electronic Engineering, Chongqing University of Posts and Telecommunications, Chongqing 400065, China

[2]School of Electronic Engineering, University of Electronic Science and Technology of China, Chengdu 610054, China

[3]Department of Electrical and Computer Engineering, Duke University, Durham, NC 27708, USA

Abstract—Time reversal imaging method based on full wave numerical technique for likely breast tumors biological tissue in the Microwave-Induced Thermo-Acoustic Tomography (MITAT) system is discussed. In this paper, the mechanism of microwave-induced thermo-acoustic is strictly described based on thermodynamics and thermo-diffusion principles; the equivalent relationship between the absorbed microwave energy distribution of the biological tissue and the induced thermo-acoustic source distribution is used as the basis of the imaging algorithm. Due to its unique noise suppression feature and the stability of the algorithm, the Time Reversal Method (TRM) based on the Pseudospectral Time-Domain (PSTD) technique is applied to image heterogeneous phantom tissues from low Signal-to-Noise-Ratio (SNR) thermo-acoustic signals. Thereafter, an integrated MITAT prototype system is presented to obtain the thermo-acoustic signals from some biologic tissue with millimeter scale. The proposed TRM method is based on PSTD technique produced two-dimensional images, presented to study the performances of the MITAT in terms of contrast and resolution. These images prove predominant advantages in both contrast and resolution compared with conventional microwave and ultrasound imaging systems for malignant tumor detection. Based on the current results, our TRM-PSTD MITAT system provides evidence to predict breast tumor in an early stage and millimeter scale.

* Corresponding author: Guoping Chen (chengp@cqupt.edu.cn).

1. INTRODUCTION

Breast cancer is the most common malignancy in women and the second leading cause of female cancer mortality [1]. Early diagnosis is the key to survive from breast cancer [2]. As a safe, comfortable, and sensitive method, Microwave-Induced Thermo-Acoustic Tomography (MITAT) is an attractive technology for early breast cancer detection. This system is based on the thermo-acoustic phenomenon, i.e., acoustic sensors can detected the mechanical wave generated by the rapid absorption of thermo-energy [3]. Several research groups, notably Kruger's group [4] and Wang's group [5], have extended the microwave-induced thermo-acoustic (MITA) mechanism to produce encouraging tomographical images for biological tissues. Inspired by the results in biological tissues imaging, other research groups [6–8] proposed potential applications of MITAT in biomedical imaging. In a MITAT system, the biological tissue radiates ultrasonic waves since the microwave energy causes tissues' thermo-elastic expansion. MITAT technology perseveres the union advantages both microwave imaging and ultrasound imaging. When a microwave pulse irradiates the biologic tissue, the image generated by a MITAT system has higher contrast than the one generated by a conventional ultrasound system. This advantage comes from high electrical conductivity contrast due to the significantly different sodium concentrations, fluid contents and electrochemical properties in different tissues, especially between the normal soft tissue and malignant tumor [9]. On the other hand, the MITAT image has higher resolution than the conventional microwave imaging, because the ultrasound wavelength in the received acoustic signals is several orders of magnitude shorter than the electromagnetic wavelength in microwave imaging technology. Furthermore, as the MITAT system utilizes non-ionizing microwave pulse radiation, it causes less health hazard to human body compared with an X-ray imaging system [10].

Two technological difficulties affect the imaging performance of a MITAT system. The first one is to detect the weak ultrasound signals with a high signal-to-noise ratio (SNR), and the ultrasound signals are affected by the microwave pulse feature. Therefore, the design of a suitable microwave pulse source, in particular its peak power, center frequency and the pulse width, and is important to achieve this target. Secondly, inverse algorithms can affect the performance of image reconstruction in a heterogeneous tissue. In a few inverse algorithms, Time Reversal Mirror (TRM), based on wave propagating and array signal processing methods, has found many successful applications in ultrasound imaging [11, 12]. Due to its effectively

suppresses system noise, spatial-temporal matched filtering property, and its finite-frequency imaging ability, it will be employed into our system.

In this paper, in order to enhance tumor mimic target contrast and resolution, we designed a powerful MITAT system to obtain high quality signals. A full-wave TRM by pseudospectral time-domain (PSTD) technique is proposed to image the targets in a heterogeneous biological tissue. The structure of this paper is as follows: Section 2 formulates the microwave-induced thermo-acoustic procedure based on thermo-dynamics and thermo-conduction mechanism in order to provide critical design principle for MITAT system. We deduce a linear relationship between the absorbed microwave energy and the induced thermo-acoustic source distribution in the tissue. This interesting founding maps the tumors microwave absorbing characteristics into receiving signals. This mapping relationship simplifies the images explanation for tumor symptom. A powerful and robust TRM technology is discussed in Section 3. Section 4 implements the TRM method by using high efficient PSTD technique. PSTD has two promising benefits. One is to conveniently model large-scale heterogeneity. In the same time, PSTD method accurately describes the thermo-acoustic wave propagation in the biologic tissue. Section 5 introduces our integrated prototype MITAT system. To validate the MITAT technique, two porcine muscle tissue cubes with millimeter scale in cross-section are used to mimic the tumor in female breast. We implement the corresponding MITAT image reconstruction and discuss the critical performance of full-wave TRM by PSTD.

2. MICROWAVE-INDUCED THERMO-ACOUSTIC MECHANISM BASED ON THERMO-DYNAMICS AND THERMO-DIFFUSE PRINCIPLES

The microwave-induced thermo-acoustic phenomenon includes two processes: first, the incident microwave energy is absorbed to produce thermal deposition in the biologic tissue; consequently, an acoustic wave is generated due to thermal expansion in the tissue. To facilitate a quantitative analysis, we consider the problem based on the following simplifying assumptions: the irradiated media are assumed to be electrically and elastically homogeneous and isotropic; acoustic attenuation is neglected since its value is small in the biologic tissue.

2.1. The MITAT Model Based on Thermo-dynamic Physics

Consider a small cube in an elastic medium with a unit volume heated by incremental thermal source. σ_{ki} is stress tensor components on the surface of the cube. The relationship between the stress components and the particle displacement vector is governed by Newton's second law of motion,

$$\sum_{k=1}^{3} \frac{\partial \sigma_{ki}}{\partial k} = \rho \frac{\partial^2 u_i}{\partial t^2} \quad i = 1, 2, 3, \tag{1}$$

where u_i is the i-th component of the displacement vector, ρ the density of the cube, $i, k = 1, 2, 3$, or equivalently x, y, z in a Cartesian coordinates. The strain components $\varepsilon_{i,k}$ are functions of the displacement vector u_i as

$$\varepsilon_{ik} = \frac{1}{2} \left(\frac{\partial u_i}{\partial k} + \frac{\partial u_k}{\partial i} \right) \quad i, k = 1, 2, 3. \tag{2}$$

The stress tensor $\sigma_{i,k}$ in the thermo-acoustic process can be expressed by the strain tensor $\varepsilon_{i,k}$ and the thermal expansion through the generalized Hooke's law:

$$\sigma_{ik} = 2R_T \left(\varepsilon_{ik} + \frac{q}{1 - 2q} e \delta_{ik} - \frac{1 + q}{1 - 2q} a T \delta_{ik} \right), \tag{3}$$

where R_T is the torsional rigid, q the Poisson's ratio, e the volume expansion ratio, that is $e = \sum_{k=1}^{3} \varepsilon_{k,i}$, $i = 1, 2, 3$, T the temperature distribution function, $\delta_{i,k}$ the Kronecker delta function, and a the coefficient of the thermal diffusivity, which is proportional to the thermal conductivity factor λ,

$$a = \frac{\lambda}{\rho \cdot c_v}, \tag{4}$$

where c_v is the isobaric thermal capacity. To clearly describe the thermo-acoustic procedure, we only consider the normal directions for simplification, so $k = i$, $\delta_{i,k} = 1$; $e = 3\varepsilon_{i,i}$ and Equation (3) can be rewritten as

$$\sigma_{ii} = 2R_T \left(\varepsilon_{ii} \frac{1 + q}{1 - 2q} - \frac{1 + q}{1 - 2q} a T \right). \tag{5}$$

Combining Equations (1), (2) and (5), we obtain

$$\sum_{i=1}^{3} \frac{\partial^2 \sigma_{ii}}{\partial i^2} - \frac{\rho}{2R_T} \frac{1 - 2q}{1 + q} \frac{\partial^2 \sigma_{ii}}{\partial t^2} = \frac{\rho}{2R_T} a \frac{\partial^2 T}{\partial t^2}, \tag{6}$$

where c is the ultrasound velocity, and $c^2 = \frac{2(1+q)}{1-2q}\frac{R_T}{\rho}$. The observed ultrasonic wave is the surface stress tensor mapped into normal direction. This relationship is express by

$$p_i = \sigma_{ii} \cdot \widehat{n}_i. \tag{7}$$

Using $\sum\limits_{i=1}^{3}\frac{\partial^2 \sigma_{ii}}{\partial i^2} = \Delta\sigma_{ii}$, where "$\Delta$" stands for Laplacian operator, Equation (6) can be rewritten as:

$$\Delta p_i - \frac{1}{c^2}\frac{\partial^2 p_i}{\partial t^2} = \frac{\lambda}{2R_T}\frac{1}{c_v}\frac{\partial^2 T(\vec{r}',t)}{\partial t^2} \tag{8}$$

2.2. The Thermo-acoustic Solution under the Thermal Conduction Situation

Equation (8) describes that the thermo-acoustic pressure wave is a function of the temperature T. Obviously, the temperature T is governed by the thermal conduction and diffuse function,

$$\Delta T\left(\vec{r}',t\right) + \frac{h(\vec{r}',t)}{\lambda} = \frac{1}{c_k}\frac{\partial T\left(\vec{r}',t\right)}{\partial t}, \tag{9}$$

where c_k is thermo-diffusion coefficient. The heating function can be written in terms of microwave irradiation by

$$h\left(\vec{r}',t\right) = -Re\left(\nabla \cdot \vec{P}\right), \tag{10}$$

where $\vec{P} = \frac{1}{2}\vec{E} \times \vec{H}^*$ is the poynting vector. $\vec{E}$ is the electrical field, $\vec{H}$ the magnetic field in biologic tissue, and superscript $*$ denotes complex conjugation. Generally, since the duration time of microwave irradiating pulse is transient, the diffuse term $\Delta T(\vec{r}',t) \approx 0$. So the simplified function (9) is substituted into Equations (6) and (8), and we arrive at

$$\Delta p_i - \frac{1}{c^2}\frac{\partial^2 p_i}{\partial t^2} = \frac{1}{2R_T}\frac{c_k}{c_v}\frac{\partial h\left(\vec{r}',t\right)}{\partial t}, \tag{11}$$

The solution of this equation is then obtained by the Green's function in time domain [13],

$$p_i\left(\vec{r},t\right) = \frac{1}{2R_T}\frac{c_k}{4\pi c_v}\iiint\limits_{|\vec{r}-\vec{r}'|=t\cdot c}\frac{d\vec{r}'}{|\vec{r}-\vec{r}'|}\frac{\partial}{\partial t'}h\left(\vec{r}',t'\right), \tag{12}$$

where $\vec{r}'$ denotes source coordinates, while $\vec{r}$ denotes receive coordinates. The integration volume is a sphere defined by $|\vec{r} - \vec{r}'| = t \cdot c$. If we define the heating function $h(\vec{r}', t') = I_0 \eta(t') \cdot \varphi(\vec{r}')$, ($I_0$ is the peak amplitude, $\eta(t')$ is the profile, and $\varphi(\vec{r}')$ is the absorbed distribution of irradiating microwave pulse energy), and $\eta(t') \approx \delta(t')$ for the width of the irradiating microwave pulse can be neglected. The ultrasonic pressure wave close to the source is proportional to $\varphi(\vec{r}')$. This pressure wave is observed so close to thermo-acoustic source that it should be distinguished with usual measured ultrasonic pressure wave. It is denoted as $p_{i0}(\vec{r}')$, so the relationship between $p_{i0}(\vec{r}')$ and $\varphi(\vec{r}')$ is

$$p_{i0}(\vec{r}') \propto \varphi(\vec{r}') \quad t = 0+, \tag{13}$$

where subscript '+' of 0+ means the moment after heating completion. This proportion relationship between the ultrasonic pressure wave source and the absorbed microwave energy distribution is important since we can transform the MITAT problem involving $\varphi(\vec{r}')$ into the problem resolving acoustic source $p_{i0}(\vec{r}')$ equivalently.

3. TRM TECHNIQUE IN HETEROGENEOUS MEDIA

Consider MITAT imaging environment: the received low SNR signals in a MITAT system and the ultrasonic wave's propagation in heterogeneous tissue media. We reconstruct the image by using the time reversal method (TRM) technique under these situations.

3.1. The Principle of TRM

TRM is based upon the reciprocity principle, which is derived from even order wave equations. Figure 1 illustrates forward and backward procedures of time reversal method principle.

Consider a thermo-acoustic source p_{i0}. It is defined by a Gaussian pulse and locates at $\vec{r}_s$, we have

$$p_{i0}(t)|_{\vec{r}_s} = -\frac{d}{dt}\left(\frac{1}{\sqrt{2\pi\sigma_t^2}} e^{-i\omega_c t} e^{-\frac{t^2}{2\sigma_t^2}}\right) = \frac{i\omega_c + t/\sigma_t^2}{\sqrt{2\pi\sigma_t^2}} e^{-i\omega_c t} e^{-\frac{t^2}{2\sigma_t^2}}, \tag{14}$$

where ω_c is the center frequency, σ_t the width of the Gaussian pulse in time domain, $BW = 2\pi/\sigma_t\omega_c$ the relative bandwidth of the ω_c, i the imaginary unit, and the corresponding form in frequency domain is,

$$\widehat{p}_{i0}(\omega) = \int_{-\infty}^{+\infty} p_{i0}(t)|_{\vec{r}_s} e^{i\omega t} dt = i\omega e^{-\frac{\sigma_t^2(\omega-\omega_c)^2}{2}}. \tag{15}$$

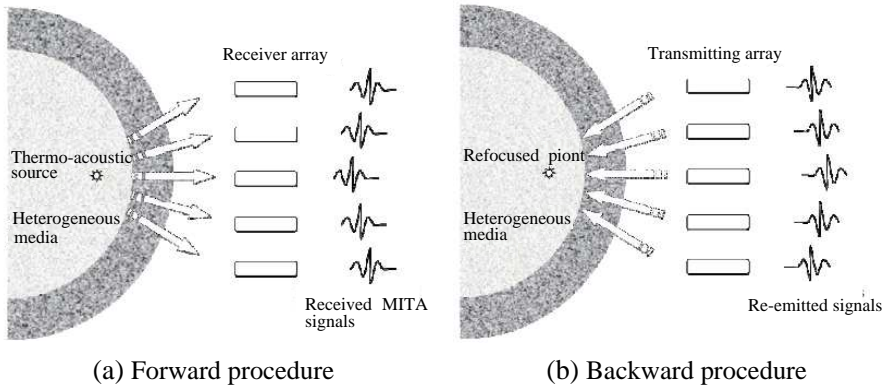(a) Forward procedure   (b) Backward procedure

Figure 1. Time reversal method principle. (a) Forward wave propagation generated by a thermo-acoustic source and received by an ultrasound array in time domain. (b) Received signals with the time reversed sequences are re-emitted into the media and refocused at the original source position.

The forward propagating procedure in Figure 1(a) can be described as,

$$s_p\left(\vec{r}_p,\ \vec{r}_s,t\right) = p_{i0}(t)|_{\vec{r}_s} \otimes G\left(\vec{r}_p,\vec{r}_s,t\right)$$

$$= \frac{1}{2\pi}\int_{-\infty}^{+\infty} \widehat{p}_{i0}(\omega)\cdot\widehat{G}\left(\vec{r}_p,\vec{r}_s,\omega\right)e^{-i\omega t}d\omega, \quad (16)$$

where symbol $\otimes$ means convolution. $\widehat{G}(\vec{r}_p,\vec{r}_s,\omega)$ is the Green's function with a source located at $\vec{r}_s$ and an observation point positioned at $\vec{r}_p$, and satisfies the wave function,

$$\nabla^2\widehat{G}(\vec{r}_p,\vec{r}_s,\omega) + k^2n^2(\vec{r})\widehat{G}(\vec{r}_p,\vec{r}_s,\omega) = -\delta(\vec{r}_p - \vec{r}_s), \quad (17)$$

where $k = \omega/c_0$, c_0 means the average ultrasonic velocity value in the heterogeneous media, and the mass density is assumed uniform in the media. The index function $n(\vec{r})$ can be defined to describe the distribution of the difference of the real velocity with respect to the average sound velocity,

$$n(\vec{r}) = \frac{c_0}{c(\vec{r})}. \quad (18)$$

The backward propagation, named as time reversal and a

procedure depicted in Figure 2(b), can be formulated as

$$s_T\left(\vec{r}_f,\vec{r}_p,t\right) = \frac{1}{2\pi}\int_{-\infty}^{+\infty} e^{-i\omega t}\widehat{p}_{i0}(\omega)\widehat{\Gamma}^{TR}\left(\vec{r}_f,\vec{r}_s,\omega\right)d\omega$$

$$\widehat{\Gamma}^{TR}\left(\vec{r}_f,\vec{r}_s,\omega\right) = \sum_{p=1}^{N}\widehat{G}^*\left(\vec{r}_f,\vec{r}_p,\omega\right)\cdot\widehat{G}\left(\vec{r}_p,\vec{r}_s,\omega\right)$$

,   (19)

where $\vec{r}_f$ is the refocusing point produced by the procedure of the time reversal (TR) and N the total number of the ultrasound transducers (UT). $\widehat{\Gamma}^{TR}(\vec{r}_f,\vec{r}_s,\omega)$ is the system function defined by TR procedure. Since in the TR procedure the received signals are re-emitted into the media along the forward propagating track just like the light reflected by a mirror, this technique is named time reversal mirror (TRM) in some literatures. After all, the power of TR is not restricted to use the receiver in a line or a plane. We focus on the procedure of time reversal, and consider it a good method for imaging. So if it will not conflict with time reversal mirror define, we use the same abbreviated form TRM for the time reversal method.

Generally, measured signals are polluted by various noises in a MITAT system, so the received signals in forward procedure should be modified as

$$s'_p(t) = s_p(t) + n(t), \tag{20}$$

where $n(t)$ is an additive white noise function. Equation (19) is then modified by Equation (20),

$$s'_T\left(\vec{r}_f,\vec{r}_s,t\right) = s_p\left(\vec{r}_p,\vec{r}_s,-t\right)\otimes G\left(\vec{r}_f,\vec{r}_p,t\right) + n(\vec{r}_p,\vec{r}_s,-t)\otimes G\left(\vec{r}_f,\vec{r}_p,t\right)$$

$$= p_{i0}(t)|_{\vec{r}_s}\otimes R\left(\vec{r}_f,\vec{r}_p,t\right) + n(\vec{r}_p,\vec{r}_s,-t)\otimes G\left(\vec{r}_f,\vec{r}_p,t\right), \tag{21}$$

where $R(\vec{r}_f,\vec{r}_p,t)$ is the autocorrelation function of $\Gamma^{TR}(\vec{r}_f,\vec{r}_s,t)$. For the ultrasonic wave $p_{i0}(t)|_{\vec{r}_s}$ propagating through the medium defined by the Green's function $R(\vec{r}_f,\vec{r}_p,t)$ and the received signals propagating again this medium in the reversed time sequence, the refocused point is enhanced N times due to the in-phase accumulation by the TR procedure, while the noise does not have this characteristic. In fact, the maximum of the refocused function s'_T can be obtained at $\vec{r}_f = \vec{r}_s$ due to the function $R(\vec{r}_f,\vec{r}_p,t)$. This character of the TRM technique usually is called spatial-temporal filtering.

4. TRM IMPLEMENTED BY PSTD

The core of the TRM is the system function $\Gamma^{TR}(\vec{r}_f,\vec{r}_s,t)$. The exact Green's function is usually unavailable by an analytical

method if the medium is heterogeneous, so a numerical method is necessary. However, conventional numerical methods such as the finite-difference time-domain (FDTD) and finite-element time-domain (FETD) methods have difficulty in solving such large-scale problems in MITAT, because the dimensions of the problem consume large memory and long computing time due to hundreds of wavelengths in each direction. In this paper, PSTD method [14] is employed to solve the forward problem in a TRM procedure. PSTD is a fast high-order time domain method with global accuracy as demonstrated in [15], and the PSTD method can give high computation efficiency for the Green's function of complex biologic tissue.

In order to use the perfectly matched layer (PML) as an absorbing boundary condition in the PSTD method, we rewrite the MITAT Equation (8) into first-order partial differential equations for particle velocity and pressure fields,

$$\begin{aligned} \frac{\partial \vec{v}}{\partial t} &= -\frac{1}{\rho}\nabla p \\ \frac{\partial p}{\partial t} &= -K\nabla \cdot \vec{v} \end{aligned}, \tag{22}$$

where $K = \rho c^2$, $\vec{v}$ is the particle velocity vector equal to $\frac{\partial u_i}{\partial t}$. In the two-dimensional case, the numerical Green's function can be obtained by discretizing Equation (22) into N nodes in orthogonal coordinates. Here $N = Nx \times Ny$, Nx, Ny are total nodes along x and y directions, respectively. We have

$$\frac{\partial W}{\partial t} = f(W), \quad W \equiv (v_x, v_y, p)^T$$
$$f(W) = \left(-\frac{1}{\rho}\frac{\partial p}{\partial x}, -\frac{1}{\rho}\frac{\partial p}{\partial y}, -K\left(\frac{\partial v_x}{\partial x} + \frac{\partial v_y}{\partial y}\right)\right)^T, \tag{23}$$

where superscript 'T' means matrix transpose, v_x, v_y are the velocity components of $\vec{v}$ along x, y directions.

In the Fourier PSTD method [16], the spatial derivatives in the first-order partial differential equations in (23) are calculated using the Fast Fourier Transform (FFT) and Inverse Fast Fourier Transform (IFFT) algorithms. Because of its global high order characteristics, a much smaller sampling density is used compared to the traditional FDTD method. For example, for a moderate problem of several wavelengths, the FDTD method requires over 20 points per wavelength (PPW) to guarantee the numerical dispersion error smaller than 1%, while the PSTD only requires about 3 PPW. Therefore, this advantage of the PSTD method is significant for our larger scale biological tissue imaging problems.

Assume that $\widehat{u}(k)$ is the spectral domain form of $u(x)$ generated by FFT and that k is the wave number (spatial Fourier variable), then $ik\widehat{u}(k)$ is the spectral domain form of $\frac{d}{dx}u(x)$, where i is the imaginary unit also. The steps of obtaining the spatial derivatives in the PSTD method are summarized as:

1) The spectral domain sequence $\widehat{u}_0, \widehat{u}_1, \widehat{u}_2, \ldots, \widehat{u}_{N-1}$ are generated by the FFT at the nodal points;
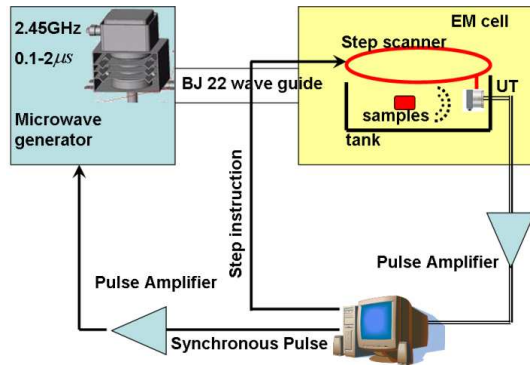

Figure 2. MITAT system setup. The prototype MITAT system consists of five subsystems. First, the microwave generator is used to generate a microwave pulse with a carrier frequency of 2450 ± 50 MHz. The pulse width, pulse repetition frequency (PRF), and peak power are adjustable. From the generator, a microwave pulse is transmitted to the tissue sample holder through a BJ22 rectangular waveguide with a $108\,\text{mm} \times 54\,\text{mm}$ cross section. Secondly, the measurement platform set in the electromagnetic shielding (microwave cell) box in which the microwave pulse is transmitted into the tissue and the induced ultrasound is collected. The tissue holder is made by polypropylene plane. To avoid the rapid loss of ultrasound in air, mineral oil is used as a coupling liquid between the ultrasound transducer and the tissue. Thirdly, a computer controlled step scanner based on MD-2 (ARRICK Company) control system is used to control the shifting of the ultrasound transducer. Fourthly, the data collection system consists of an ultrasound transducer (Panametrics V323, the center frequency is 2.25 MHz, the -3 dB bandwidth is about 1.5 MHz) and a preamplifier. The piezoelectric signal obtained by the ultrasound transducer is amplified by the preamplifier before it is sent to the PCI data acquisition card. Finally, a 5 V digital synchronous signal generated by the data acquisition card is amplified by a pulse amplifier to trigger the microwave pulse generator.

2) $ik\widehat{u}(k)$ can be obtained by $\widehat{u}_0, \widehat{u}_1, \widehat{u}_2, \ldots, \widehat{u}_{N-1}$ multiplied by the wave number, that is, $0 \cdot \widehat{u}_0, \pi \cdot \widehat{u}_1, 2\pi \cdot \widehat{u}_2, \ldots, (N-1)\pi \cdot \widehat{u}_{N-1}$;

3) $\frac{d}{dx}u(x)$ at the nodal points can be obtained by the IFFT of the $ik\widehat{u}(k)$ data.

Finally, the resulting wave fields $u(x)$ can be obtained by time integration for ordinary differential equation.

5. EXPERIMENTAL SYSTEM SETUP AND MITAT IMAGING

5.1. The Prototype MITAT System and Typical MITAT Signals

We developed a MITAT prototype to detect thermo-acoustic signals. Figure 2 shows a schematic diagram of our MITAT experimental system. The setup of this system is partially benefited from the other research group [17–19]. The flexible scan mode and adjustable microwave peak value and width of the modulated pulse are the prominent features of this prototype MITAT system.

In MITAT experiments, microwave pulses with 500 Hz PRF, 30 kW peak power and 1.0 μs pulse width along the x direction are irradiated into two porcine muscle tissue cubes. All the samples and the UT are immersed into the mineral oil to alleviate the ultrasonic attenuation in the air, as shown in the photograph in Figure 4. In our system, we use the receiving transducer. It transforms the thermo-acoustic press into voltage signals.

Figure 3(a) is a snapshot of two porcine muscle tissue samples held by two polypropylene branches, and the branches can rotate powered by a step motor. Through wavelet threshold de-noising method [20], Figure 3(b) gives two voltage signals generating with and without tissue samples.

Figure 3(b) gives the type MITAT signals generated by the biological tissue. The green solid line is the recorded MITAT signals for the samples. For the purpose of comparison, the blue dotted line is recorded signals without samples. Obviously, our system can give above 15 dB SNR MITAT signals based on the microwave power and preamplifier configure.

5.2. Results and Discussion

We reconstruct the 2D image for the samples given in Figure 4. The total discretized number of cells N is 1024×1024. Unit cell size is 0.1484 mm, so the image area is 152 mm × 152 mm. 8 cells of

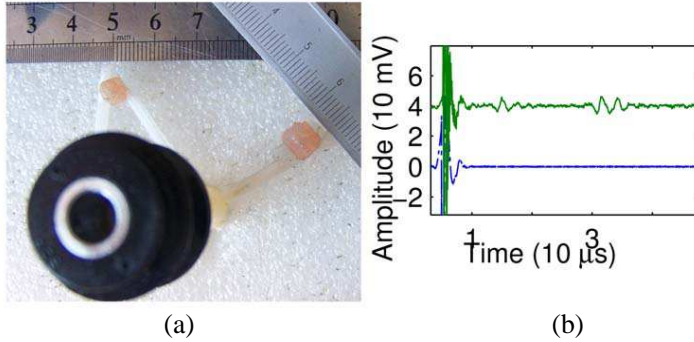(a)   (b)

Figure 3. (a) The top view of the porcine muscle tissue objects. The cross-section size of smaller one is 5 mm long and 3 mm wide, and the larger one is 7 mm long and 3 mm wide, respectively. The sample size of the smaller cube is about 5 mm long and 3 mm wide; the larger sample is 7 mm long and 3 mm wide. Both cubes are about 15 mm high located at two separate polypropylene branches. The distance between the two cubes is about 45 mm. The samples can be rotated in an increment of 0.9 degree per step in the x-y plane around the rotary axis along the z direction, which is driven by a step motor. The UT scanner samples 360 degrees, so the total scan number is 400. The UT is fixed at 38 mm away from the rotary axis. The sampling ratio of the data acquisition card is set at 50 MHz. The time-domain sampling number at each location is 5000 to a maximum time of 100 µs, and the ultrasound signals at each step is averaged 256 times and amplified 1000 times before being sampled. (b) Signals recorded by the receiver (UT) at the 1st step with (top green line) and without (bottom blue line) the tissue samples. The signal in marked 1 area is disturbed by microwave pulses. The marked 2 area is the one sample generated; the marked 3 area is another one. The voltage signal is recorded at the 1st step. The max value is 46 mV. The peak is at 64 µs.

the perfectly Matched Layer (PML) are used at each computational boundary to absorb outgoing waves. The time step is 20 ns, same as the actual sampling step. The PSTD based TRM is applied with the same configuration as described in Section 4. Figure 4(a) is a grayscale map of all the 400 recorded signals versus time. Figure 4(b) shows the TRM imaging result.

Figure 4(c) is an enlarged picture of the left object from Figure 4(b). For the microwave-induced thermo-acoustic derived from the thermal difference between the heated tissue and background, the edges of the cubes are the main features in the reconstructed images.
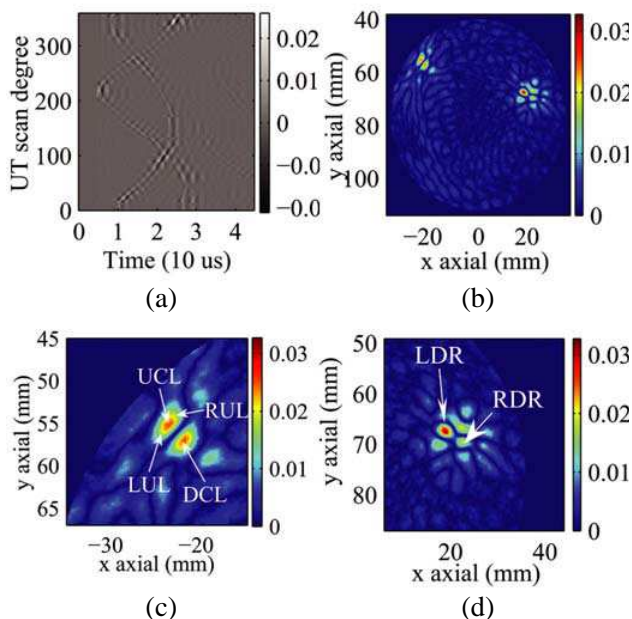
Figure 4. The map of all received signals versus time and image generated by TRM based on the PSTD method. The two curves in Figure 4(a) clearly show the two target samples. (b) is the normalized image obtained by Full-wave TRM Full-wave TRM by PSTD method. The two targets are identified. (c) Enlarged images of the targes. The high lighted red area is the high hydrous biological tissue imaging results. Due the MITAT signals only generated by the edge of the media with outstanding electromagnetic energy absorption parameter, so the RUL and DCL in (c), the same as the (d), are the two edge of a target. To quantity the dimension of the imaged targets, marking two maximum value points in (c) as UCL and DCL, the location of them are (−23.85, 54.48) and (−21.77, 57). The unit is mm both in x and y axial direction. And the width of each high lighted area is defined by RUL, LUL. RUL and LUL is the −3 dB of the maximum value point of the UCL or DCL.

In Figure 4(c), the strongest points marked UCL (Upper edge Center of the Left sample) and LCL (Lower edge Center of the Left sample) are located at (−23.85, 54.48) and (−21.77, 57) mm, so the thickness of the left object is 3.27 mm; the −3 dB width determined by the strongest point is marked LUL (Left Upper center of the Left sample) and RUL (Right Upper center of the Left sample) for the upper edge is located

Table 1. Comparison of the length and width parameters between
the actual values and reconstructed values.

UCL	DCL	Thick	Actual thickness
$(-23.85,\ 54.48)$	$(-21.77,\ 57)$	3.27 mm	3 mm
LUL	RUL	Wide	Actual width
$(-25.48,\ 56.85)$	$(-22.21,\ 52.84)$	5.17 mm	5 mm

at $(-25.48,\ 56.85)$ and $(-22.21,\ 52.84)$ mm, so the length of the left
object is 5.17 mm. The right object can be analyzed similarly.

Table 1 shows the length and width parameters comparison
between the actual values and those obtained from Figure 4(c). The
central positions of the objects determined by the four centers are
$(-22.96,\ 56.11)$ and $(21.17,\ 67.54)$ mm, respectively, so the distance of
the two objects is 45.59 mm. This is very close to the actual distance
of 45 mm. The contrast defined by the strongest point over the average
background noise is larger than 45 dB.

Figure 4 demonstrates the capability of MITAT with full-wave
TRM by the PSTD method. Due to the length limitation, some
comparisons between a MITAT system with presented method and
other applications for the tumor targets are not presented there,
including systematic comparison between MITAT and ultrasound
system for the high hydrous tissue imaging [19]. The high hydrous
state is an outstanding feature for the tissue with early deteriorate
characters. Others compare between the TRM based on PSTD
and back project (BP) method for the same recorded MITAT
signals [21, 22].

6. CONCLUSIONS

Breast cancer is one of the highest fatal diseases for the female,
which can be observed at age from teens to eighties of them. In
terms of the cancer tissue, it has such as chemic and physical change
compared with the normal tissue even at the early stage. For a new
technique of the MITAT system to image the tumor in breast, three
aspects of research results are presented in this paper. Firstly, the
microwave-induced thermo-acoustic procedure is strictly studied based
on thermo-dynamics and thermo-diffuse principles, the theoretical
forms involving electromagnetism, mechanical, and thermodynamics
physics. This theoretical framework is the fundamental for the
systematic design of a MITAT system, and the parameters include

microwave power and waveform design, preamplifier and signals preprocess. Also given by the theoretical results, the proportional relationship between the microwave energy deposition of the biological tissue and the induced thermo-acoustic source distribution is obtained, which explains the equivalently transform between the electromagnetic feature of the tumor and the easy observed thermo-acoustic sources problem. Secondly, an integral prototype MITAT system is presented, and the experimental details are presented to obtain the high SNR signals. By our system, above 15 dB SNR MITAT receiver signals can be obtained by a narrow microwave pulses irradiating source. This pulse mode can effectively decrease the total electromagnetic energy, which enables the MITAT system according to the FCC safety requirement. And the circle scan mode is configured to generate the biggest scan angle, from which, the generated images can give most geometry information of the tumor. Lastly, as the TRM technique has great potential in noise suppression, TRM based on the pseudo-spectral time domain method is introduced into MITAT. In order to validate the performance of TRM in the imaging of MITAT and emphasize that the method can be applied to an actual MITAT system, biological tissue images generated by an MITAT prototype system are studied. It has been shown that the TRM images have very high contrast and resolution. For our experimental system configure, above 20 dB contrast can be obtained, and images with an order of millimeter resolution can be achieved. Higher resolution can be expected through improving the bandwidth of the MITAT system. Decreasing the irradiating microwave power may be future improvement if considering for safe issue. After achieving these future works, devising a more practical prototype for breast cancer detection and analyzing the effect of the actual background medium can be expected.

ACKNOWLEDGMENT

REFERENCES

1. Jemal, A., R. Siegel, J. Xu, and E. Ward, "Cancer statistics," *A Cancer Journal for Clinicians*, Vol. 60, No. 5, 277–300, 2010.

2. Veronesi, U., N. Cascinelli, L. Mariani, M. Greco, R. Saccozzi, A. Luini, M. Aguilar, and E. Marubini, "Twenty-year follow-up of a randomized study comparing breast-conserving surgery with

radical mastectomy for early breast cancer," *N. Engl. J. Med.*, Vol. 347, 1227–1232, 2002.

3. Guo, T. C., W. W. Guo, and L. E. Larsen, "Microwave-induced thermo-acoustic effect in dielectrics and its coupling to external medium — A thermo dynamical formulation," *IEEE Trans. Microwave Theory Tech.*, Vol. 32, No. 8, 835–843, 1984.

4. Kruger, R. A., W. L. Kiser, D. R. Reinecke, G. A. Kruger, and R. L. Eisenhart, "Thermoacoustic computed tomography of the breast at 434 MHz," *IEEE MTT-S International Microwave Symposium Digest*, Vol. 2, 591–595, 1999.

5. Xu, M. and L. V. Wang, "RF-induced thermo-acoutic tomography," *Proceedings of the Second Joint EMBS/BMES Conference*, 1211–1212, 2002.

6. Zeng, L., D. Xing, H. Gu, and D. Yang, "A fast microwave-induced thermoacoustic tomography system for imaging of biological tissues," *Fourth International Conference on Photonics and Imaging in Biology and Medicine, Proc. of SPIE*, Vol. 6047, 60470K, 2006.

7. Anastasio, M. A., K. Wang, J. Zhang, G. A. Kruger, D. Reinecke, and R. A. Kruger, "Improving limited-view reconstruction in photoacoustic tomography by incorporating a priori boundary information," *Proc. of SPIE*, Vol. 6856, 68561B.1, 2008.

8. Lim, K. H., J. H. Lee, and Q. H. Liu, "Thermoacoustic tomography forward modeling with the spectral element method," *Medical Physics*, Vol. 35, No. 1, 4–12, 2008.

9. Joines, W. T., Y. Zhang, C. Li, and R. L. Jirtle, "The measured electrical properties of normal and malignant human tissues from 50 to 900 MHz," *Am. Assoc. Phys. Med.*, Vol. 21, 547–551, 1994.

10. Paulsen, K. D. and P. M. Meaney, *Alternative Breast Imaging,* Springer Press, 2006.

11. Fink, M., "Time reversal of ultrasonic fields. I. Basic principles," *IEEE Transactions on Ultrasonics, Ferroelectrics, and Frequency Control,* Vol. 39, No. 5, 555–567, 1992.

12. Fouque, J. P. and G. Papanicolaou, *Wave Propagation and Time Reversal in Randomly Layered Media,* Springer Press, 2007.

13. Botrth, D. E. and C. A. Cain, "Theoretical analysis of acoustic signal generation in materials irradiated with microwave energy," *IEEE Trans. Microwave Theory Tech.*, Vol. 25, No. 11, 944–953, 1997.

14. Liu, Q. H., "The PSTD algorithm: A time-domain method combining the pseudospectral technique and perfectly matched

layers," *J. Acous. Soc. Am.*, Vol. 101, No. 5, 3182–3182, May 1997.

15. Liu, Q. H., " The PSTD algorithm: A time-domain method requiring only two cells per wavelength," *Microwave and Optical Technology Letters*, Vol. 15, No. 3, 158–165, 1997.

16. Wojcik, G., B. Fomberg, R. Waag, L. Carcione, J. Mould, L. Nikodym, and T. Driscoll, "Pseudo-spectral methods for large-scale bioacoustic models," *IEEE Ultrasonics Symposium*, Vol. 2, 1501–1507, Oct. 1997.

17. Kruger, R. A., L. Kiser, Jr, D. R. Reinecke, G. A. Kruger, and R. L. Eisenhart, "Thermoacoustic computed tomography of the breast at 434 MHz," *IEEE MTT-S International Microwave Symposium Digest*, Vol. 2, 591–594, 1999.

18. Nasoni, R. L., S. C. Liew, P. G. Halverson, and T. Bowen, "Thermoacoustic images generated by a 2450 MHz portable source and applicator," *IEEE 1985 Ultrasonics Symposium*, 899–904, 1985.

19. Xu, M. and L. V. Wang, "Pulsed-microwave-induced thermoacoustic tomography: Filtered backprojection in a circular measurement configuration," *Medical Physics*, Vol. 29, No. 8, 1661–1670, 2002.

20. Chen, G.-P., W.-B. Yu, Z.-Q. Zhao, Z.-P. Nie, Q.-H. Liu, "The design of electromagnetically induced thermo-acoustic system and the signal processing using wavelet analysis with a soft thresholding method," *Chinese of Journal Electronics*, Vol. 36, No. 6, 1130–1134, 2008.

21. Chen, G., Z. Zhao, W. Gong, Z. Nie, and Q.-H. Liu, "The development of the microwave-induced thermo-acoustic tomography prototype system," *Chinese Science Bulletin*, Vol. 52, No. 12, 1786–1789, 2009.

22. Chen, G. P., Z. Q. Zhao, Z. P. Nie, and Q. H. Liu, "A computational study of time reversal mirror technique for microwave-induced thermo-acoustic tomography," *Journal of Electromagnetic Waves and Applications*, Vol. 22, No. 12, 2191–2204, 2008.